

Article

Not peer-reviewed version

Variable-Sized Green Mussel Shell Waste: A Sustainable Approach to Artificial Sand Production

[Pimthong Thongnopkun](#)*, Worachai Roubroumlert, Chutiparn Lertvachirapaiboon

Posted Date: 22 July 2025

doi: 10.20944/preprints2025071646.v1

Keywords: green mussel shell; aragonite; calcite; artificial sand; sustainability



Preprints.org is a free multidisciplinary platform providing preprint service that is dedicated to making early versions of research outputs permanently available and citable. Preprints posted at Preprints.org appear in Web of Science, Crossref, Google Scholar, Scilit, Europe PMC.

Copyright: This open access article is published under a Creative Commons CC BY 4.0 license, which permit the free download, distribution, and reuse, provided that the author and preprint are cited in any reuse.

Disclaimer/Publisher's Note: The statements, opinions, and data contained in all publications are solely those of the individual author(s) and contributor(s) and not of MDPI and/or the editor(s). MDPI and/or the editor(s) disclaim responsibility for any injury to people or property resulting from any ideas, methods, instructions, or products referred to in the content.

Article

Variable-Sized Green Mussel Shell Waste: A Sustainable Approach to Artificial Sand Production

Pimthong Thongnopkun ^{1,*}, Worachai Roubroumlert ² and Chutiparn Lertvachirapaiboon ³

¹ Faculty of Science, Burapha University, Saensuk, Chonburi 20131, Thailand

² Faculty of Gems, Chanthaburi Campus, Burapha University, Chanthaburi 22170, Thailand

³ National Nanotechnology Center, National Science and Technology Development Agency, Pathum Thani 12120, Thailand

* Correspondence: pimthong@go.buu.ac.th

Abstract

An innovative approach is presented in this article as a potential alternative for reusing discarded green mussel shells from fishing and food sectors. This technique entails the use of harmless chemicals and the consumption of energy in an efficient manner to generate shell powder of different dimensions. Fourier Transform Infrared (FTIR) spectroscopy assessed the purity of the treated shells, while X-ray Diffraction (XRD) spectroscopy examined their crystal structure. The microstructure of shell powder of different sizes was investigated using scanning electron microscopy (SEM). Furthermore, we analyzed the thermal characteristics of different sizes of crushed shell. In addition, we determined the changed surface color of the seashell before and during heat treatment, as it has a substantial impact on the ultimate product result. A diverse spectrum of particle sizes characterizes the shell powder, making it suitable for use in several industrial applications. Based on the available research regarding the benign characteristics of crushed shell particles, it is quite probable that they can be used as ecologically suitable artificial sand. Furthermore, the final part of the paper provides concrete illustrations of employing crushed shells as artificial sand.

Keywords: green mussel shell; aragonite; calcite; artificial sand; sustainability

1. Introduction

Thailand is renowned for its abundant food resources and is one of the leading countries globally in terms of food production and export, notably in the seafood industry [1,2]. Nevertheless, the primary challenge of seafood production and export lies in appreciated waste management, particularly in tourist and industrial regions, where the handling of seafood waste continues to be troublesome. In these regions, effective waste management is required due to the occurrence of unpleasant odors from spoiling seafood trash when it is not properly managed over long periods of time. Typically, this trash is allowed to undergo natural decomposition, hence exacerbating the destruction of the environment [3].

The eastern region of Thailand such as Chonburi, Rayong, Chanthaburi, and Trat are coastal areas where many residents engage in seafood harvesting and processing. These places are also notable tourist sites, drawing a large number of visitors from all over the globe, resulting in a substantial demand for seafood. Shellfish is highly sought after for its delectable flavor and exceptional nutritional advantages. The mussel is a highly popular shellfish due to its widespread availability and versatility in culinary preparations. This gives rise to the issue of accumulated mussel shell waste. Presently, the disposal of trash generated by seafood industry, particularly mussel shells, presents a substantial obstacle (Figure 1). After consuming the meat, an estimated 5 million tons of shells are discarded annually mostly through landfill, which is improper as it causes soil and water pollution, reduces soil porosity and fertility, and impedes water absorption [4,5]. Shells require a

maximum of 10 years to undergo decomposition and are not biodegradable. Moreover, the expense associated with appropriately disposing of shell trash is substantial. Local restaurant owners and shell processors stated in interviews that trash disposal often entails burying the shells. Disused shells are frequently abandoned in residential or public spaces to undergo natural decomposition, leading to olfactory pollution, causing disruptions in communities, and serving as breeding sites for disease-causing microorganisms, which could potentially affect public health. Nevertheless, because of the irregular nature of this gathering, the trash gradually builds up, resulting in unpleasant smells and problems with air pollution. In addition, the decomposition of shell debris in acidic settings results in the release of carbon dioxide, which has a substantial impact on global warming [6,7].

Due to the significant impact of shell waste on shellfish growers, sellers, and consumers, both in terms of practicality and economics, numerous research efforts have been made to convert shell waste into sustainable materials [8–10]. The scientific literature documents the utilization of several kinds of seashells for the creation of innovative biomaterials. The shells of bivalve mollusks are primarily composed of calcium carbonate (CaCO_3), which is a key component in many materials. These shells have the potential to be valuable raw material for various uses. CaCO_3 is widely recognized in industry for its versatile uses, such as being a fluxing agent in the steel industry, a filler in the polymer business, and a raw ingredient for producing mortars, plasters, refractories, glass, and additives [10–12]. The compound CaCO_3 can undergo decomposition and be converted into calcium oxide (CaO) by a process called calcination [7,10,13–15]. The outcome is contingent upon the temperature at which calcination occurs and the characteristics of the compounds prior to the shell's calcination. On the other hand, CaO has been used as a primary substance in the manufacturing of essential chemicals including sodium carbonate, calcium carbide, calcium sulfite, and calcium hydroxide, among others [10–12]. Both materials have garnered considerable attention in various applications.

The primary focus of most shellfish-based research is the investigation of the conversion of CaCO_3 to CaO through the process of fire at various temperatures. The study focused on investigating the thermal decomposition of CaCO_3 and analyzing the relationship between temperature and other factors, including lattice constants, thermal expansion coefficients, lattice strain, and crystallite size. The primary method for pretreating seashells to obtain CaO is rinsing the shells with tap water. Subsequently, acetone or mild acids were employed to eliminate organic substances from the shell. Hence, certain chemicals used in manufacturing processes may have an impact on the environment. Subsequently, the shell was subjected to boiling for a duration of 30 – 60 minutes or followed by heating for 1–4 hours at 105–120 °C, and finally pulverized to get CaCO_3 powder [10,13,16]. Once CaCO_3 is acquired, the conventional approach to handling CaCO_3 entails subjecting to CaO use high-temperature incineration prior to their utilization in other goods or small-scale industries [10,17,18]. This process necessitates the use of kilns and entails substantial energy and time consumption, yielding shell powder consisting of minute CaO particles. Consequently, it is not feasible for the local community to manage vast quantities of discarded shells independently [17–21].

This research aims to propose an alternative approach involving the extraction and refinement of CaCO_3 from green mussel shells (GS), which are the predominant form of shellfish waste in the seafood sector. The method involves creating shell powder of different sizes through an eco-friendly chemical approach to obtain CaCO_3 and CaO . It utilizes an alkaline solution to eliminate organic impurities, which may be safely discharged into the environment at the completion of the process without causing any harm to the local community. The production process is straightforward, energy-efficient, and does not necessitate heating for several hours. By employing grinding techniques, the particle size of the shell powder may be regulated, rendering it appropriate for various industrial uses. It is possible to create distinct products that are suitable for each size. Producing alternate types of different-sized CaCO_3 products could be a viable method to handle shellfish waste without resorting to incineration. Therefore, before undergoing the calcination process, the properties of CaCO_3 of each size were researched. Furthermore, we performed an analysis of the seashells' color both prior to and during thermal treatment, as the color of the seashells

significantly influences the results of the diverse products [22,23]. Moreover, it indicates the level of purity and cleanliness of the processed shells.

As an alternative to converting CaCO_3 powder into CaO , our research also investigates the calcination of various sizes of processed CaCO_3 to CaO at a temperature of 800°C . This temperature range was determined based on the calcination temperature of CaCO_3 shells, which is typically between $700\text{--}900^\circ\text{C}$. Additionally, 800°C is commonly utilized in many applications of CaCO_3 . Additionally, the purity of the processed shell powders, both non-calcined and calcined GS powder, was analyzed by FTIR spectroscopy, and the crystal structures of the shells were investigated using X-ray diffraction (XRD) techniques. Furthermore, we investigated the effect of temperature on the combustion of shells of varying sizes using thermogravimetry and differential thermal analysis (TG/DTA). This research yields useful insights that can be applied in diverse industries. In this study, we utilized waste shells for the purpose of sustainable application of artificial sand. Specific examples of the use of artificial sand made from GS smash are also mentioned in the last section of the article.



Figure 1. Seashell waste from fishing and the food industry.

2. Materials and Methods

The trash mussel shells were acquired from Bang Pra, Chonburi Province, Thailand. The shells have been subjected to a washing process using tap water to remove any external debris and impurities. The production of GS powder entailed submerging the discarded shells in a 3.00 M potassium hydroxide solution for a period of 14 days. This procedure was conducted to efficiently eradicate organic debris, decomposing compounds, and detrimental bacteria found on the outer layer of the shells. Subsequently, they were cleansed and dry in the atmosphere. The laboratory roller ball mill was employed to grind the crushed seashells into a finely powdered form. Afterwards, the crushed shell powder underwent filtration using mesh with pore diameters of 200, 60, and $20\ \mu\text{m}$ to separate and collect the sections with different particle sizes that were used in this investigation. Figure 2 depicts the thorough preparation process. The figure exhibits color photographs of waste GS and finely powdered GS powder. In order to examine the effects of different sizes of calcined crushed shell powder on appearance and structural changes, the powder was passed through various sizes of sieves and then exposed to calcination at a temperature of 800°C for 1 hour using an electric furnace. The non-calcined and calcined samples underwent investigation utilizing Scanning Electron Microscope and Energy Dispersive X-ray Spectrometer (SEM-EDS), TG-DTA analysis, XRD spectroscopy, UV-Visible spectroscopy, and ATR-FTIR spectroscopy.

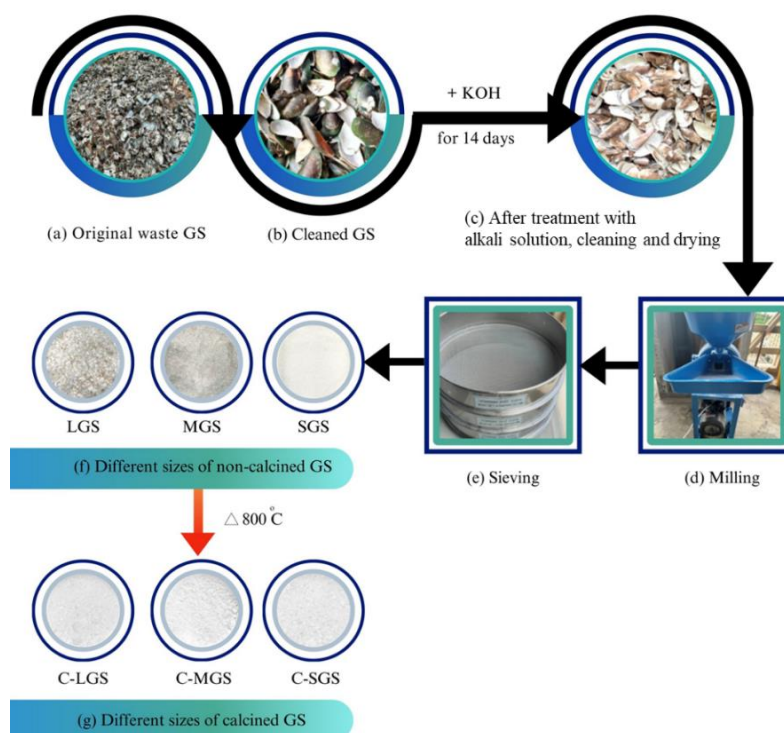


Figure 2. The pre-treatment procedure for green mussel shell (GS) powder.

The Shimadzu 2600 UV-Visible spectrophotometer was used to analyze the reflectance spectra of the samples. The measurements were conducted using reflection mode with a wavelength range of 350 nm to 800 nm. The color variations of the samples were examined using CIE $L^*a^*b^*$ color measurement. Each color index can be individually interpreted. The L^* represents the numerical value of brightness, ranging from 0 (representing black) to 100 (representing white). There is no specific numerical limit for the variables a^* and b^* . The colors will intensify as the magnitudes of a^* and b^* grow. Red represents positive a^* , whereas green represents negative a^* . Similarly, yellow represents positive b^* , while blue represents negative b^* .

The scanning electron microscopy (SEM) technique was used to investigate the surface morphology of various sizes of crushed GS using the JEOL JSM-6510A instrument. For determining the crystalline phases present in the GS powder, X-ray diffraction (XRD) patterns were obtained for each of the shells of various sizes. X-ray examinations were conducted to determine the mineralogical phases present in the GS at both room temperature and after being heated to 800 °C. In order to achieve this objective, a Bruker D8 X-Ray Diffractometer was utilized. The thermal profile measurement and weight loss during heating were measured using a simultaneous thermogravimetric analyzer (STA Instrument, NETZSCH STA 449C model).

FTIR spectroscopy was carried out using a Thermo Scientific Nicolet Summit X FTIR spectrometer. The spectra were obtained using Attenuated Total Reflectance (ATR) techniques. The ATR-FTIR spectra were acquired via the Smart Everest ATR attachment. The spectra were obtained in the mid-infrared range from 500 to 4000 cm^{-1} . Each spectrum was collected using 64 accumulations with a spectral resolution of 4 cm^{-1} . The various dimensions of GS crush were positioned on a diamond IRE and meticulous measures were implemented to ensure accurate contact. Before further examination, the observed spectra performed baseline correction.

3. Results and Discussion

3.1. Appearance and Color

Table 1 provides comprehensive comparisons of the crushed shell before and after being subjected to calcination at a temperature of 800 °C. During the process of grinding and sieving the shell, it was observed that the largest crushed green mussel shell (LGS) retained a noticeable iridescent quality from the inner layer of the shell. The medium-crushed green mussel shell (MGS) had a diminished iridescence, while the smallest crushed green mussel shell (SGS) exhibited a fine white powder that rarely appears iridescent properties. The LGS displays a blend of brownish-gray and yellow tones, mixed with white, which signifies that an alkaline environment can degrade proteins into tiny peptides, resulting in the formation of brown-colored substances [24,25]. After calcination at a temperature of 800 °C, all three shell sizes exhibited a white powdery residue that lacked iridescence and had a white appearance with a subtle yellowish-gray hue.

Table 1. Appearance and color values of different-sized GS.







Samples	Appearance (Photo)	L*	a*	b*
LGS		80.14 ± 1.92	1.65 ± 0.37	9.25 ± 1.82
MGS		77.82 ± 1.76	0.21 ± 0.12	7.96 ± 1.97
SGS		75.21 ± 1.10	0.347 ± 0.06	9.17 ± 4.82
C-LGS		87.12 ± 0.47	0.15 ± 0.03	5.98 ± 0.44
C-MGS		87.51 ± 0.00	-0.04 ± 0.00	7.06 ± 0.38
C-SGS		85.06 ± 0.63	0.07 ± 0.01	7.39 ± 0.16

Table 1 demonstrates that the L* values of all calcined samples have exhibited an increase in appearance and color. Furthermore, the a*b* values of the calcined shells shift towards a neutral value, indicating a lighter shade and a transition to white color. This corresponds to the visual appearance of the shell powder obtained from all calcined samples. The L*a*b* values demonstrate the color alteration effects prior to and following the application of heat, as depicted in Figure 3. The graph clearly shows a rise in the luminosity or L* value of each sample (Figure 3a), along with a movement towards greater negative values in the a* and b* values (Figure 3b). The calcined GS had the palest hue and the closest similarity to the white reference after calcination with 800 °C. The alteration in hue of the specimen can pertain to the phenomenon of CaCO₃ calcination. The study conducted by N. Suwannasingha et al. [10] discovered that subjecting marine shell debris to calcination at a temperature of 700 °C produces a gray hue, which progressively transitions to a lighter shade of yellow at 900 °C. The transformation of CaCO₃ into CaO can be achieved. These data exhibited a comparable pattern to our observation. Furthermore, our discovery demonstrates that

exposing shells of different sizes and initial flake characteristics to a temperature of 800 °C can uniformly transform them into CaO powder, regardless of their size.

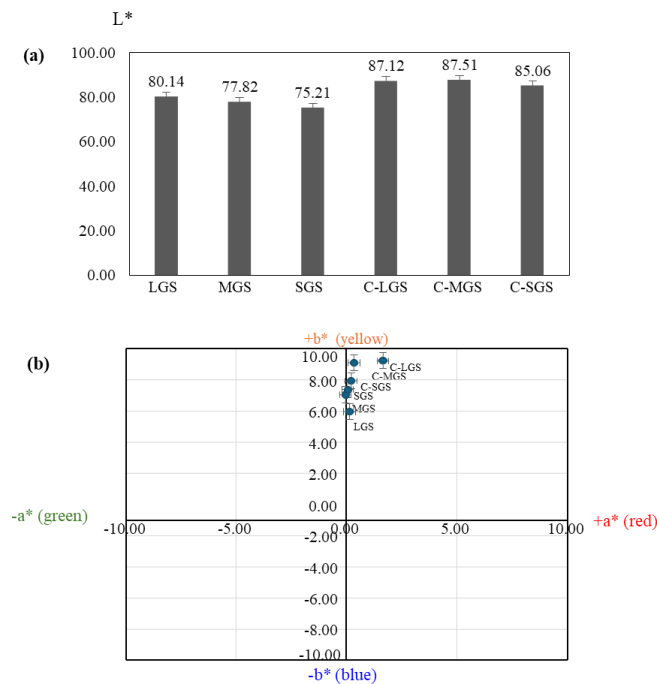


Figure 3. Color values of different-sized non-calcined and calcined GSs (a) L* and (b) a*b* diagram.

Figure 4 presents the reflection spectra of the samples. The calcined crushed shells of SGS and MGS exhibit a higher reflection percentage compared to non-calcined crushed shells. The reflectance of calcined crushed shells (C-SGS) is 1.2 times more than that of non-calcined crushed shells, while the reflectance of calcined mixed grain shells (C-MGS) is 1.8 times greater. The computation was performed using the percent reflectance value at a wavelength of 550 nm. The observed outcomes could potentially be attributed to the increased surface area of calcined crushed shells, resulting in enhanced light scattering. However, LGS has the highest reflectance due to its strong angular reflection, as mentioned in the reference by Lertvachirapaiboon [26]. This ultimately results in a higher overall reflection value.

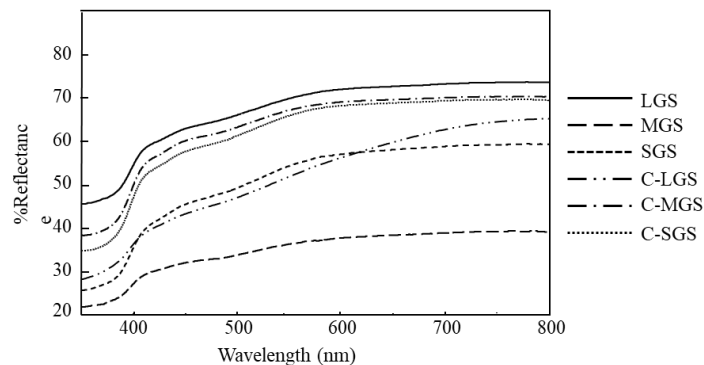


Figure 4. Reflectance spectra of different-sized non-calcined and calcined GS.

3.2. Morphology Observation by SEM-EDS

The Scanning Electron Microscope (SEM) was used to analyze the structure and shape of crushed GS of different sizes, as depicted in Figure 5. The scanning electron microscope (SEM) pictures shown in Figure 5a illustrate the LGS particles that have a plate-like structure with a size that ranges from around 1800 to 2000 microns. SEM images of MGS and SGS are depicted in Figure

5b and 5c, respectively. The shells have average diameters of approximately 400 microns and 200 microns, respectively. The SEM pictures in Figure 5d – f depict the surface of fragmented shells. The diagram illustrates the preserved structure of the mussel shell, which consists of stacked layers of plate-shaped CaCO_3 . This enables the crushed shells to possess exceptional light-reflecting characteristics [26,27]. Small fragments of aragonite plates are present on the surface of the crushed shells. The SEM images of calcined crushed shells are depicted in Figure 5g–i. Following the calcination process, CaCO_3 underwent decomposition, resulting in the release of CO_2 and subsequent decomposition of the organic matrix present in the crushed shell. The relevant data may be found in the thermal profile section. The results indicated that the crushed shell underwent fragmentation into smaller particles, whereas the surface between the CaCO_3 plates experienced sintering and fusing together [15,28]. Subsequently, a shrinking of the CaCO_3 plates was observed.

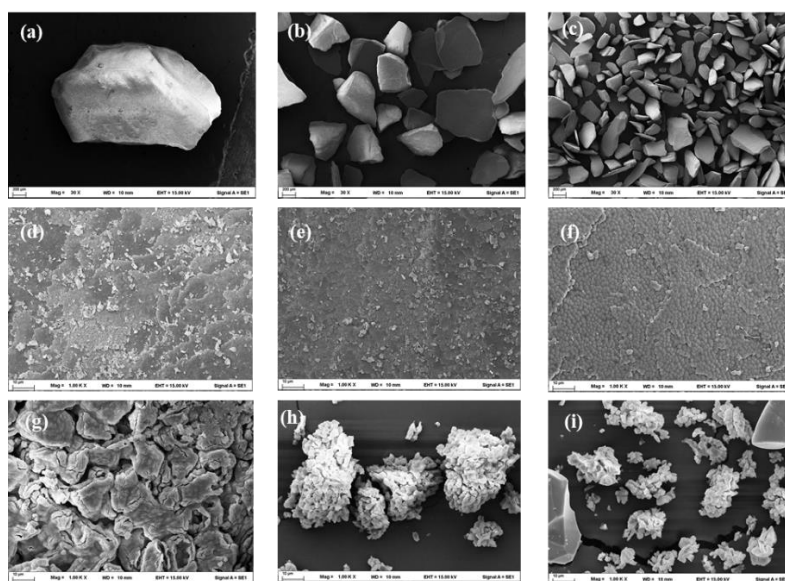


Figure 5. SEM images of crushed shell; (a) LGS; (b) MGS; (c) SGS (d) surface of LGS; (e) surface of MGS; (f) surface of SGS; (g) calcined LGS (h) calcined MGS; and (i) calcined SGS.

The elemental analysis conducted with Energy Dispersive X-ray Spectroscopy (EDS) indicated that both crushed shells and calcined crushed shells consist of calcium (Ca), carbon (C), and oxygen (O). However, the specific EDS data is not provided. The XRD analysis reveals a comprehensive composition analysis of crushed shells and calcined crushed shells.

3.3. X-Ray Diffraction (XRD) Analysis

The XRD spectrum of LGS, as shown in Figure 6a, unequivocally demonstrates the presence of the aragonite polymorph with a purity of 100%. Figure 6b and 6c display XRD spectra of MGS and SGS, correspondingly. The experimental results indicate that these shells, which are of moderate and small size, consist of a combination of calcite and aragonite polymorphs of CaCO_3 . The occurrence can be attributed to the thermal energy generated during the grinding and erosion of the shell during processing, resulting in the creation of small amounts of different crystal forms of calcite within the CaCO_3 structure. Figure 6d–f displays the X-ray diffraction spectra of the calcined powders from all three shell sizes at a temperature of 800°C. Figure 6d illustrates the result of the LGS that has undergone the most thorough calcination process. The presence of lime (CaO) appears to exist, whereas a little quantity of CaCO_3 in the form of calcite is present. In addition, the presence of portlandite (Ca(OH)_2) is indicated at trace levels, which are less than 1%. The X-ray diffraction (XRD) patterns of medium and small-sized shells after calcination, as shown in Figure 6e and 6f, reveal higher concentrations of CaO and Ca(OH)_2 compared to the larger shells. The difference can be attributed to the larger surface area of smaller broken shells, which enables them to efficiently release

heat energy and decompose at a faster rate [29,30]. Furthermore, if an atmosphere with oxidizing properties is present during the calcination process, there is an increased likelihood of CaO, carbon dioxide, or water undergoing a reaction, leading to a greater production of Ca(OH)_2 in comparison to larger shells.

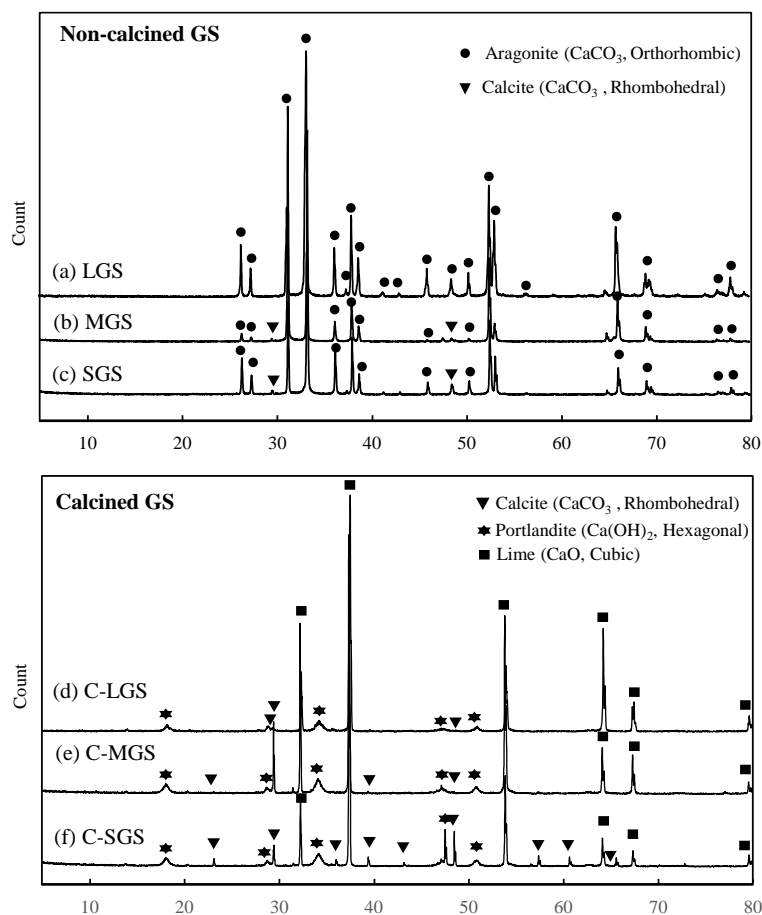


Figure 6. XRD spectra of different-sized non-calcined and calcined GS; (a) LGS; (b) MGS; (c) SGS; (d) C-LGS; (e) C-MGS; and (f) C-SGS.

3.4. Thermal Profile

In order to comprehensively investigate the thermal degradation of shells of different sizes, the organic component content was measured using TG/DTA analyzer. Figure 7 exhibits the thermogravimetric (TG) and differential thermal analysis (DTA) curves for different sizes of GS powder. All samples exhibit two clearly distinguishable thermal transitions in their DTA diagrams, which are an endothermic transition and an exothermic transition. The DTA curve of LGS powder displayed endothermic peak of heat absorption at around 275 °C and 453 °C. This peak corresponds closely to the temperature at which the organic substance on the shell undergoes fusion [14,30]. On the other hand, there is a clear exothermic process occurring at approximately 817 °C, which is linked to the thermal decomposition of CaCO_3 into CaO. Figure 7b and 7c present the TG/DTA results for MGS and SGS powder. An exothermic reaction was seen at temperatures of about 269 °C and 450 °C, indicating the decomposing of the organic component on the surface of the LGS powder. Furthermore, a thermally induced reaction occurred with a slight decrease in mass at the maximum recorded temperature of 811 °C for MGS powder and 804 °C for SGS powder. This reaction involves the decomposition of CaCO_3 into CaO. The results showed that the decomposition temperature of these powders had a slight fluctuation.

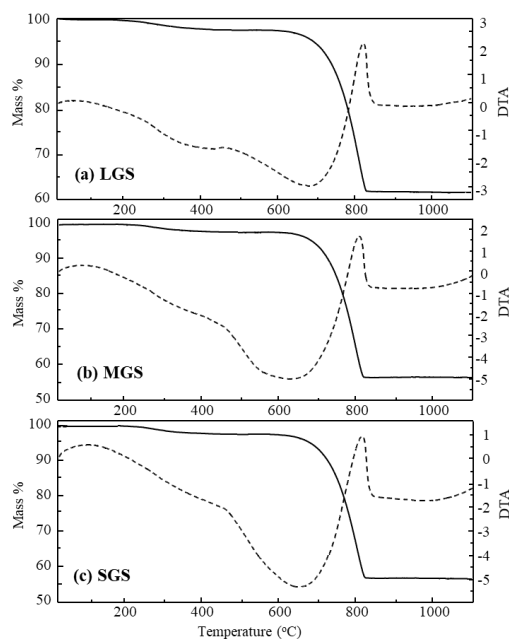


Figure 7. TG-DTA diagrams of different-sized GSs. (a) LGS; (b) MGS; and (c) SGS.

The average weight loss of all samples, due to organic decomposition, from room temperature to around 450 °C, is approximately 2.6%. Additionally, thermal analysis conducted on all variations of GS revealed that the decomposition of calcite takes place between the temperature range of 700 °C to 800 °C. The weight loss range observed in the TG curve, notably ranging from 35% to 42%, is attributed to the liberation of gaseous carbon dioxide (CO₂) [7,14,30]. The TG analysis reveals that the weight loss percentage in LGS is 35.78%, which is comparatively lower than that of MGS (41.25%) and SGS (41.33%). The DSC curve has an endothermic form between 700 °C and 800 °C, indicating that the thermal breakdown initiated slowly and then increased significantly when the temperature exceeded 750 °C. This observation is further confirmed by the analysis of X-ray diffraction (Figure 6). The X-ray diffractograms unequivocally illustrate the creation of CaO and the total absence of calcite at around 800 °C, showing the culmination of thermal degradation. The results correspond to the quantity of CaO and Ca(OH)₂ produced during the decomposition of CaCO₃, as seen in Figure 6e–f. The relationship between temperature and composition during the thermal conversion of calcite demonstrates a noticeable shift in composition or an accelerated rate of conversion at 800 °C from CaCO₃ to CaO and Ca(OH)₂ (Figure 6e–f).

3.5. FT-IR Spectroscopy

The study employed ATR-FTIR spectroscopy to evaluate the purity of GS after a green chemical procedure and to characterize the changes in functional groups in GS after calcination. Figure 8 exhibited the ATR spectra of different dimensions of crushed GS. The particular wavenumber at which the absorption peaks of LGS powder are observed are shown in Figure 7a: 700, 712, 854, 1080, 1240, 1414, 1473, 1635, and 1785 cm⁻¹ [10]. The presence of the aragonite phase is responsible for the observed peaks, as supported by the XRD data presented in Figure 6a. A band detected within the 1400–1470 cm⁻¹ range indicates the stretching of the C–O bonds in carbonate. The shell displays a prominent absorption in this area, which is a distinctive characteristic of aragonite. In addition, the LGS spectra displays a carbonate out-of-plane bending vibration at 854 cm⁻¹, and an in-plane bending vibration at 700–712 cm⁻¹ in its FTIR spectrum. Aragonite has a prominent double peak at 700 and 712 cm⁻¹, with a greater absorbance at 700 cm⁻¹ compared to 712 cm⁻¹. The spectra of GS exhibited an absorption peak at 1080 cm⁻¹, which suggests the existence of aragonite. This unique band is undetectable within the calcite structure. This result confirms the existence of aragonite in the GS,

which corresponds to the results of the XRD examination. Furthermore, the spectra display a clearly defined, narrow peak at 1780 cm^{-1} , indicating the elongation of the C=O bond. In addition, there is a minimal absorption of triplet bands within the range of $2500\text{--}2650\text{ cm}^{-1}$ and $2800\text{--}2950\text{ cm}^{-1}$ that correspond to brownish-gray color in their appearance (Table 1). These bands are caused by the existence of residual organic molecules in the broken shell. In addition, a weak band at 3300 cm^{-1} , which indicates the absorption of OH groups, was seen. This observation provides convincing evidence of the dimensions of the non-calcined shell.

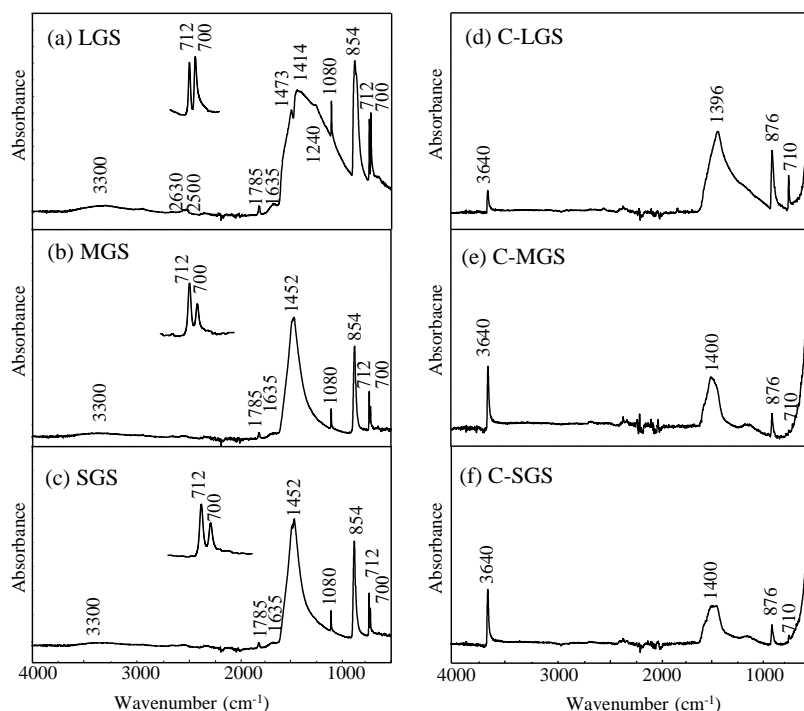


Figure 8. FTIR spectra of different-sized non-calcined and calcined GS; (a) LGS; (b) MGS; (c) SGS; (d) C-LGS; (e) C-MGS; and (f) C-SGS.

The FT-IR spectra of MGS and SGS show a similar pattern, which is characteristic of CaCO_3 at specific wavenumber of 700, 712, 840, 854, 1230, 1400, 1635, 1785, 2500, and 2630 cm^{-1} (Figure 8b and 7c) [10]. Unlike LGS (Figure 8a), these samples have a single peak at 1452 cm^{-1} , which is indicative of calcite. Moreover, when analyzing the two peaks at 700 and 712 cm^{-1} , it is evident that the absorbance at 712 cm^{-1} , which represents the existence of calcite, is higher than the absorbance at 700 cm^{-1} , which indicates the existence of aragonite. The MGS and SGS spectra both display an absorption peak around 1080 cm^{-1} , which is comparable to the LGS spectra. This peak indicates the coexistence of aragonite and calcite in the structure. This discovery offers further substantiation of the existence of aragonite in the clam shells, confirming the outcomes derived from the XRD study.

The ATR spectra of all samples after calcination at a temperature of 800°C are shown in Figure 8d–f. Every spectrum has an identical spectral pattern. The FT-IR spectra of the calcined powders indicated the presence of carbonate ions (CO_3^{2-}) through the observation of C-O stretching bands, specifically at wavenumbers of 1400, 874, and 712 cm^{-1} [31]. The absence of the absorption peak at 700 cm^{-1} can be ascribed to the breakdown of aragonite. The peak at 853 cm^{-1} experiences a transition to 876 cm^{-1} , indicating a unique vibration related to the conversion of CaO from the calcite phase to the calcite form of limestone. The conclusion was made based on the observation that the shell possessed bands with the same characteristics as limestone (CaO) at specific wavelengths: 1400 cm^{-1} (asymmetric stretching), 872 cm^{-1} (out-of-plane bending), and 712 cm^{-1} (in-plane bending) [10,32]. Moreover, the absorption peaks at $2800\text{--}2900\text{ cm}^{-1}$, $2600\text{--}2700\text{ cm}^{-1}$, and 3350 cm^{-1} , which are caused by organic matter and the OH group of a little amount of water adsorbed on the surface, were

completely removed after calcination. In all spectra, a distinct peak at 3640 cm^{-1} is detected, which corresponds to the O-H stretching of calcium hydroxide or portlandite. Portlandite is produced by the interaction of CaO with water or atmospheric moisture [33,34] according to the Eq (1):



Following the process of calcination, the CaCO_3 underwent a conversion into CaO and CO_2 . CaO can undergo a chemical reaction with water or moisture in the atmosphere, resulting in the formation of Ca(OH)_2 . Those results are consistent with the previous data reports [35]. Therefore, the ATR-FTIR spectra demonstrates that all GS crushes are characterized by cleanliness and the main component of the calcined aragonite form of GS produces calcium. The correlation between the XRD and FT-IR results verified that all samples achieved complete conversion of CaCO_3 to CaO at the calcination temperature of $800\text{ }^\circ\text{C}$.

3.6. Potential Future Implementation

At present, there is a noticeable inclination towards adopting substitute materials for sand obtained from organic materials, namely recycling used resources. Artificial sand serves as a viable substitute for natural sand, finding application in diverse fields. As we have demonstrated in the above experimental results, all GS particle sizes are clean and non-toxic. Different sizes are suitable for different applications. Larger particles of GS display a robust, aesthetically pleasing, and lustrous surface, rendering them well-suited for ornamental applications. Medium-sized GS particles can be used as artificial sand, while the finest particles, although less glossy, have a soft texture that is non-irritating. This indicates a high potential for use as artificial sand instead of silicon dioxide sand (SiO_2) in various applications.

In certain cases, exotic pet care, which is continuously gaining popularity, can substitute medium and large-sized GS in this article for SiO_2 . Some exotic animals might ingest SiO_2 sand, which poses a risk because it is indigestible and may cause blockages in the digestive system, irregular defecation, fecal retention, and constipation [36], especially in animals with complex or sensitive digestive systems. For example, reptiles such as lizards and snakes, as well as amphibians like frogs and salamanders, may face digestive problems if they accidentally ingest SiO_2 sand. Using CaCO_3 powder from GS as a substitute for SiO_2 sand is a safer option in some cases because CaCO_3 is digestible in the digestive systems of certain animals, particularly those that require calcium, such as reptiles and amphibians. Calcium is also beneficial for building bones and eggshells. Many animals, including turtles and lizards, can break down CaCO_2 in their digestive systems, thereby supplementing their bodies with calcium. CaCO_2 does not carry the same risk of gastrointestinal obstruction as SiO_2 , which is not digestible and may cause blockages.

Our clean medium-sized GS powder can serve as a substrate in terrariums, vivarium, and aquariums for aquaculture and decoration, thereby creating an environment that closely mimics the natural habitat of these animals. Cleanliness is also a key characteristic of artificial sand for aquaculture. This type of artificial sand helps to balance pH, cleanliness, and safety for aquatic animals. Additionally, certain shades are designed to accurately create a genuine atmosphere. By using synthetic sand of different sizes for specific purposes, particles with a diameter of less than 1 millimeter can be utilized for aquatic plants and soft-bodied invertebrates, such as snails and shrimp.

In addition, our medium and large crushed GS can be used as artificial sand in small Zen gardens and can also be mixed into home decor products by incorporating them into concrete to produce raw concrete pots, vases, bricks, and other decorative materials. The large aragonite surface's luster, which resembles glitter, will enhance the products' shine.

The small-sized GS is suitable for use as a substitute material for artificial sand for children, which is mostly made from silica sand, including finely crushed limestone or marble. Gypsum or certain types of plaster used in children's toys may cause allergic reactions in children, especially if there are additional chemicals that could trigger allergies, such as preservatives or synthetic dyes. Allergic symptoms may include itching rashes, swelling, or respiratory issues. For this application, GS that is finely ground and free from chemical residues is suitable because it is non-toxic, has

hygienic properties, and is available in various particle sizes. Finely ground GS also provides very fine particles with a smooth surface, which is gentle on the skin, thereby reducing the likelihood of skin irritation in children.

We focus on the valorization of GS waste, which constitutes a significant environmental challenge not only in Thailand but across multiple geographical regions globally. The transformation of this marine waste stream into value-added products offers a threefold benefit: (1) remediation of accumulated waste, (2) reduction of future waste generation, and (3) creation of economic opportunities for local communities. Moreover, our methodology enables the production of sand with varying particle size distributions through a controlled mechanical grinding process, thereby facilitating diverse application potentials. This approach presents a sustainable circular economy solution for developing alternative construction materials, particularly artificial sand, addressing both environmental concerns and resource scarcity in the construction industry.

4. Conclusions

The utilization of green mussel shells (GS) derived from seafood processing waste, subjected to chemical treatment protocols, facilitates the production of purified shell powder with controlled particle size distributions. The resulting powder exhibits pH neutralization properties, maintains high purity standards, and ensures safety compliance while requiring minimal energy input during manufacturing processes. Particle size modulation of the shell powder can be systematically controlled to meet specific application requirements. The optical reflectance characteristics of mussel shell powder demonstrate a positive correlation with particle size, exhibiting higher reflectance values for larger particles and progressively diminishing reflectance as particle dimensions decrease.

Prior to thermal treatment, the shell powder presents an off-white to brownish coloration. Upon calcination at 800°C, crystallographic analysis reveals that larger mussel shells predominantly exhibit aragonite crystal structure, whereas smaller particles demonstrate calcite configuration. However, thermal processing at this temperature induces complete color transformation to white across all particle size fractions. The calcination process facilitates the structural conversion of both aragonite and calcite polymorphs to lime (CaO) and portlandite [Ca(OH)₂]. Post-calcination analysis confirms the absence of impurities across all particle size categories.

The size-graded CaCO₃ particles derived from GS demonstrate versatility comparable to synthetic sand alternatives, finding applications across multiple industries including aquaculture systems, ornamental horticulture, specialized pet substrates, and therapeutic spa treatments. Furthermore, the CaO product obtained through 800°C calcination maintains superior purity and whiteness characteristics, rendering it suitable for diverse industrial applications requiring high-grade calcium oxide.

Author Contributions: Conceptualization, P.T., W.R. and C.L.; methodology, P.T., and C. L.; investigation, P.T. and C.L.; data curation, P.T., and C.L.; writing—original draft preparation, P.T.; writing—review and editing, C.L.; visualization, P.T and W.R.; supervision, P.T.; project administration, C.L.; funding acquisition, P.T. All authors read and approved of the final manuscript.

Funding: This research was supported by the Faculty of Science, Burapha University; Thailand Science Research and Innovation (TSRI); the National Science Research and Innovation Fund (NSRF) (Fundamental Fund: Grant No. 3.3/2568) and the Science Innovation Facility, Faculty of Science, Burapha University (SIF-IN-49300011).

Institutional Review Board Statement: Not applicable.

Informed Consent Statement: Not applicable.

Data Availability Statement: All the data are presented in the main text. Any other data are available from the corresponding author upon reasonable request.

Acknowledgments: This work was financially supported by (i) Burapha University (BUU), (ii) Thailand Science Research and Innovation (TSRI), (iii) National Science Research and Innovation Fund (NSRF) (Fundamental

Fund: Grant no.3.3/2568) and Faculty of Science, Burapha University. The authors would like to thank the Science Innovation Facility, Faculty of Science, Burapha University (SIF-IN-49300011) and Microscopic Center at the Faculty of Science, Burapha University and Scientific and Technological Research Equipment Centre (STREC) at Chulalongkorn University for instrument supports.

Conflicts of Interest: The authors declare they have no competing interests.

Abbreviations

The following abbreviations are used in this manuscript:

GS	Green mussel shell
LGS	Large-crushed green mussel shell
MGS	Medium-crushed green mussel shell
SGS	Smallest crushed green mussel shell

References

1. U.S. Department of Agriculture (USDA). Thailand's food and restaurant trends in 2022. Report no. TH2022-0018, 10 March. Global Agricultural Information Network; 2022.
2. U.S. Department of Agriculture (USDA). Seafood report. Report no. TH8067, 5 August. Global Agricultural Information Network; 2018.
3. Venugopal, V.; Sasidharan, A. Seafood industry effluents: Environmental hazards, treatment and resource recovery. *J. Environ. Chem. Eng.* **2021**, *9*(2), 104758.
4. Department of Fisheries, Ministry of Agriculture and Cooperatives. Marine fisheries management plan of Thailand 2020–2022. Ministry of Agriculture and Cooperatives, Thailand; 2022.
5. Department of Fisheries, Ministry of Agriculture and Cooperatives. Statistics of marines shellfish culture survey 2021. Report no. 5/2022, July. Fishery Statistics Group, Fisheries Development Policy and Planning Division, Thailand; 2022.
6. Lagos, N.A.; Benítez, S.; Duarte, C.; Lardies, M.A.; Broitman, B.R.; Tapia, C.; Tapia, P.; Widdicombe, S.; Vargas, C.A. Effects of temperature and ocean acidification on shell characteristics of *Argopecten purpuratus*: implications for scallop aquaculture in an upwelling-influenced area. *Aquac. Environ. Interact.* **2016**, *8*, 357–370.
7. Wongsanmai, S. Characterization of calcium oxide derived from cockle shells for carbon dioxide capture. *SNRU J. Sci. Technol.* **2018**, *10*(1), 32–36.
8. Zhan, J.; Lu, J.; Wang, D. Review of shell waste reutilization to promote sustainable shellfish aquaculture. *Rev. Aquacult.* **2021**, *14*(1), 477–488.
9. Uzcátegui, L.U.M.; Vergara, K.; Bordes, G.M. Sustainable alternatives for by-products derived from industrial mussel processing: A critical review. *Waste. Manag. Res.* **2022**, *40*(2), 123–138.
10. Suwannasingha, N.; Kantavong, A.; Tunkijjanukij, S.; Aenglong, C.; Liu, H.-B.; Klaypradit, W. Effect of calcination temperature on structure and characteristics of calcium oxide powder derived from marine shell waste. *J. Saudi. Chem. Soc.* **2022**, *26*(2), 101441.
11. Seo, J.; Lee, J.G.; Thriveni, T.; Baek, C.S.; Ahn, J.-W. Improving recycled fiber by applying in-situ aragonite calcium carbonate formation process. *Mater. Trans.* **2014**, *55*(2), 378–382.
12. Gopi, S.; Subramanian, V.K.; Palanisamy, K. Aragonite–calcite–vaterite: A temperature influenced sequential polymorphic transformation of CaCO₃ in the presence of DTPA. *Mater. Res. Bull.* **2013**, *48*, 1906–1912.
13. Jamilludin, A.J.; Dinatha, I.J.H.; Supii, A.I.; Partini, J.; Kusindarta, D.L.; Yusuf, Y. Chemical and morphological analysis of calcium oxide (CaO) powder from sea urchin (*Diadema setosum*) shell. *Eng. Chem.* **2023**, *3*, 37–43.
14. Kalinkin, A.M.; Kalinkina, E.V.; Zalkind, O.A.; Makarova, T.I. Chemical interaction of calcium oxide and calcium hydroxide with CO₂ during mechanical activation. *Inorg. Mater.* **2025**, *41*(10), 1073–1079.

15. Tian, X.K.; Lin, S.C.; Yan, J.; Zhao, C.Y. Sintering mechanism of calcium oxide/calcium carbonate during thermochemical heat storage process. *Chem. Eng. J.* **2022**, *428*, 131229.
16. Chen, B.; Peng, L.; Zhong, H.; Zhao, Y.; Meng, T.; Zhang, B. Improving the mechanical properties of mussel shell aggregate concrete by aggregate modification and mixture design. *Case Stud. Constr. Mater.* **2023**, *18*, e02017.
17. Jung, U-I.; Kim, B-J. Characteristics of mortar containing oyster shell as fine aggregate. *Materials.* **2022**, *15*(20), 7301.
18. Khiri, M.Z.A.; Matori, K.A.; Zainuddin, N.; Abdullah, C.A.C.; Alassan, Z.N.; Baharuddin, N.F.; Zaid, M.H.M. The usability of ark clam shell (*Anadara granosa*) as calcium precursor to produce hydroxyapatite nanoparticle via wet chemical precipitate method in various sintering temperature. *Springerplus.* **2016**, *5*(1), 1206.
19. Liao, Y.; Wang, X.; Wang, L.; Yin, Z.; Da, B.; Chen, D. Effect of waste oyster shell powder content on properties of cement-metakaolin mortar. *Case Stud. Constr. Mater.* **2022**, *16*, e01088.
20. Liu, H-Y.; Wu, H-S.; Chou, C-P. Study on engineering and thermal properties of environment-friendly lightweight brick made from Kinmen oyster shells & sorghum waste. *Constr. Build. Mater.* **2020**, *246*, 118367.
21. Owuamanam, S.; Cree, D. Progress of bio-calcium carbonate waste eggshell and seashell fillers in polymer composites: A review. *J. Compos. Sci.* **2020**, *4*(2), 70.
22. Pham, V.T.; Phan, N.H.; Luo, G-F.; Lee, H-Y.; Nguyen, D.Q.A. The application of calcium carbonate CaCO_3 and titania TiO_2 for color homogeneity and luminous flux enhancement in PC-LEDs. *J. Adv. Eng. Comp.* **2021**, *5*(2), 75–82.
23. Gueli, A.; Bonfiglio, G.; Pasquale, S.; Troja, S.O. Effect of particle size on pigments colour. *Color. Res. Appl.* **2016**, *42*(2), 236–243.
24. Álvarez-Viñas, M.; Rodríguez-Seoane, P.; Flórez-Fernández, N.; Torres, M.D.; Díaz-Reinoso, B.; Moure, A.; Domínguez, H. Subcritical water for the extraction and hydrolysis of protein and other fractions in biorefineries from agro-food wastes and algae: a Review. *Food Bioprocess Tech.* **2020**, *14*(3), 373–387.
25. Zhang, Z.; Wang, B.; Chen, J.; Adhikari, B. Modification of plant and algal proteins through the Maillard reaction and complex coacervation: mechanisms, characteristics, and applications in encapsulating oxygen-sensitive oils. *Sustain. Food Technol.* **2024**, *2*(3), 567–593.
26. Lertvachirapaiboon, C.; Parnklang, T.; Pienpinijtham, P.; Wongravee, K.; Thammacharoen, C.; Ekgasit, S. Selective colors reflection from stratified aragonite calcium carbonate plates of mollusk shells. *J. Struct. Biol.* **2015**, *191*(2), 184–189.
27. Xu, J.; Zhang, G. Unique morphology and gradient arrangement of nacre's platelets in green mussel shells. *Mater. Sci. Eng. C.* **2015**, *52*, 186–193.
28. Yamasaki, N.; Weiping, T.; Jiajun, K. Low-temperature sintering of calcium carbonate by a hydrothermal hot-pressing technique. *J. Mater. Sci. Lett.* **1992**, *11*, 934–936.
29. Mohamed, M.; Yusup, S.; Maitra, S. Decomposition study of calcium carbonate in cockle shell. *J. Eng. Sci. Technol.* **2012**, *7*(1), 1–10.
30. Karunadasa, K.S.P.; Manoratne, C.H.; Pitawalab, H.M.T.G.A.; Rajapakse, R.M.G. Thermal decomposition of calcium carbonate (calcite polymorph) as examined by in-situ high-temperature X-ray powder diffraction. *J Phys Chem Solids.* **2019**, *134*, 21–28.
31. Charlena; Maddu, A.; Hidayat, T. Synthesis and characterization of hydroxyapatite from green mussel shell with sol-gel Method. *Jurnal. Kimia. Valensi.* **2022**, *8*(2), 269–279.
32. Ferraz, E.; Gamelas, J.A.F.; Coroado, J.; Monteiro, C.; Rocha, F. Exploring the potential of cuttlebone waste to produce building lime. *Mater. Constr.* **2020**, *70*(339), e225.
33. Nugroho, B.S.; Wahyuni, D.; Asri, A.; Mustafa, U. Effect of calcination temperature on the powder of freshwater snail shells (*Sulcospira testudinaria*) properties. *POSITRON.* **2023**, *13*(2), 158–165.
34. Karaoui, M.; Hsissou, R.; Alami, M.; Assouag, M. Physico-chemical characterization of snail shells powder prepared by mechanochemical processes and thermal treatment. *J. Met. Mater. Miner.* **2023**, *33*(2), 139–147.
35. Shankar, V.; Jambulingam, R. Waste crab shell derived CaO impregnated Na-ZSM-5 as a solid base catalyst for the transesterification of neem oil into biodiesel. *Sustain. Environ. Res.* **2017**, *27*(6), 273–278.

36. Mans, C. Clinical update on diagnosis and management of disorders of the digestive system of reptiles, *J. Exot. Pet Med.* **2013**, *22*, 141-162.

Disclaimer/Publisher's Note: The statements, opinions and data contained in all publications are solely those of the individual author(s) and contributor(s) and not of MDPI and/or the editor(s). MDPI and/or the editor(s) disclaim responsibility for any injury to people or property resulting from any ideas, methods, instructions or products referred to in the content.